Sensors and Actuators A 309 (2020) 111964

Contents lists available at ScienceDirect

Sensors and Actuators A: Physical

journal homepage: www.elsevier.com/locate/sna

Enhancing acceleration of droplets moving on inclined surfaces by decreasing density of projection for microfluidic devices to transport droplets

Satomitsu Imai*, Shingo Oshima, Ryohei Sakuma

Department of Precision Machinery Engineering, College of Science and Technology, Nihon University, 7-24-1, Narashinodai, Funabashi, 274-8501, Japan

ARTICLE INFO

Article history:
Received 15 September 2019
Received in revised form 18 February 2020
Accepted 16 March 2020
Available online 30 April 2020

Keywords:
Acceleration
Microdroplet
Area ratio of projection
Projection density
Viscosity
Surface tension

ABSTRACT

In the fields of medicine, biotechnology, and chemical analysis, the need often arises to transport a very small amount of liquid. The characteristics of sliding acceleration by inclined surfaces with arrayed micro-pillars were examined. This work related to the surface technology required for the actuator of a microfluidic device such as a μ-TAS to improve the movement of droplets. The ease of movement of the droplets, 5 to 20 μl as the target volume, was evaluated by the acceleration in a relatively short distance from the beginning of movement. The acceleration of the droplets was also measured when the viscosity and surface tension of the droplet were changed. The size of the projection, made of silicon, was 15 μm square (height: about 20 μm). The area ratio of the projection was mainly used to evaluate the surface performance. The area ratio was varied from 0.9% to 25%. The relationship between the area ratio and the sliding acceleration when the inclined angle was 20° was measured. The water droplets slide almost had a spherical shape for a low area ratio. The sliding acceleration increased with a decrease in the area ratio; when the area ratio was approximately less than 2%, it was close to the theoretical sliding acceleration with no friction. When the area ratio was less than 1 %, the water droplets fell down between the projection gaps. When the area ratio was more than approximately 21%, the acceleration was greatly reduced. Lowering the area ratio was also useful for increasing the sliding acceleration, even for a solution with high viscosity or low surface tension. It was confirmed that the acceleration was significantly enhanced by decreasing the projection density.

1. Introduction

Technologies for transporting small amounts of droplets are often required in the fields of medicine, biotechnology, and chemical analysis such as μ-TAS [1–4]. A very small amount of a droplet is difficult to be transported because the influence of the surface forces becomes larger. For practical usage, the velocity of a droplet sliding down an inclined surface is important. Therefore, this work investigated the characteristics of sliding acceleration in a method of using inclined surfaces with micro-pillars to develop an actuator.

Many studies have been conducted on transporting a small amount of liquid droplets. Their research focus could be roughly classified thus: (a) static characteristics of water repellency for a flat surface with chemical treatment or surface roughness or surface projections, and (b) dynamic characteristics such as sliding angle, sliding velocity, and acceleration for an inclined surface with surface roughness or projections.

As for studies on (a), thin films of water repellent substances, such as silane, alkyl, and hydrophobic polymers were formed on the surface [5–8]. The wettability and the behavior of water droplets on horizontal substrates were examined [9,10]. Studies for moving droplets by electrostatic force (electret) [11–14] and acoustic waves [15] were also conducted. Studies on (b) centered on the relationship between the length of the contact line of three phases (substrate, droplet, and atmosphere) and the hydrophobicity of the substrate [16], observation of the sliding behavior of droplets [17–20], examination of frictional force [21], and forming hydrophobic and hydrophilic patterns on the surface to facilitate sliding performance of droplets [22].

Conventional studies reported that it was difficult to obtain superhydrophobicity by using only chemical treatment [5,6]. Therefore, many studies on the improvement of water repellency have used surface roughness or projections according to the Wenzel and Cassie–Baxter models [23,24]. Decreasing the length of the

* Corresponding author.
E-mail address: imai@eme.cst.nihon-u.ac.jp (S. Imai).

https://doi.org/10.1016/j.sna.2020.111964
0924-4247/

contact line of the three phases is effective for making the droplet slide easily because the length possibly decreases by providing projections to the surface [16,25]. Studies have been conducted on the effect of surface roughness; for example, sliding angle of water droplets on the water repellent surface [25–27], the effectiveness of the surface roughness of the nanometer level to ease droplet slippage [28], and micro and nano-patterned superhydrophobic polymers [29–31]. This work adopted the method of using projections. Studies on the contact angle, adhesiveness, and friction of water droplets in relation to the size, pitch, and height of the projections as a surface texture were conducted [32–34]. These studies aimed to control the hydrophobicity and sliding velocity of the water droplet. This work is closely related to them. It was also reported that the surface roughness on the nanometer level affected the ease of droplet slippage [35].

It is desirable to be able to control the sliding velocity of a droplet easily. The objective of this work was to clarify the relationship between the area ratio of the projection and the acceleration quantitatively, to enhance the sliding acceleration close to the sliding acceleration without friction. The target volume was 5 to 20 μl (approximately 2 to 3.5 mm in diameter). The features of this work are as follows. There have been few studies that measured the acceleration of droplets by changing the gap and size of projections. This work mainly used the area ratio of the projections to show the density of projections, which was defined as the area of all projections divided by the total surface area. The gap of the projections was also used to investigate the characteristics of the acceleration. The acceleration was also investigated when the hydrophobicity and hydrophilicity of the substrate were changed.

For the dynamic characteristics, studies have been conducted on the relationship between the sliding acceleration of the droplet and the dynamic contact angle on the hydrophobic surface [36–39], the influence of pillar surface fraction and pillar height by using molecular dynamics [40], and the slipping behavior of a droplet on a slope with texture; for example, slippage on a superhydrophobic surface with texture or on the modified surface [41,42]. It was clear that when the droplet slides down an inclined surface, there is a sliding mode and a rolling mode [41]. Sliding mode and rolling mode have different accelerations. Therefore, the behavior of the droplet during moving was investigated in terms of the acceleration as well as observation by high-speed camera

Hysteresis has been reported as an influential factor in relation to the sliding acceleration of droplets; for example, there have been studies reporting that a correlation existed between the acceleration of the droplet and the dynamic contact angle in the case of a fluorine silane-coated surface [38]; in addition, constant acceleration was generated, and the behavior of the droplet was mainly slipping when the static contact angle was great [41]. In this work, the acceleration was calculated using the Furmidge and Carre models [44,45] and compared with the measured values.

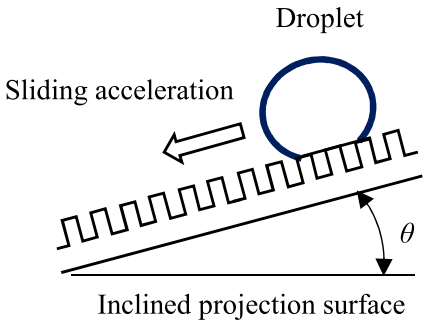

Fig. 1. Improvement of transporting a small droplet by decreasing density of the projection formed on the inclined surface.

Table 1
Specifications of micro-pillars.

Cross-section	Square 15 μm × 15 μm
Area ratio (%)	0.9, 1.4, 2.0, 3.1, 5.3, 7.5, 10, 15, 21, 25
Gap (μm)	140, 110, 90, 70, 50, 40, 32, 24, 18, 15
Height (μm)	20 (±5)

Studies on the effect of viscosity of droplet were conducted [43]. There is a study indicating that viscosity affected the sliding velocity when the sliding velocity exceeded approximately 0.1 m/s [33]. The influence of the surface tension has not been investigated much. In this work, the relationship between the viscosity or the surface tension and the acceleration was investigated. The range of the viscosity and the surface tension where this method could enhance the sliding acceleration was investigated. In addition, the relationship between the surface tension and the projection gap was examined in terms of whether the droplet with low surface tension was formed on the projection surface.

2. Material, processing, and experiment method

Fig. 1 shows the method of transporting small droplets in this work. The water-repellent performance was improved by confining the air between the projections [24]. This work relates to the surface technology required for the actuator in a microfluidic device such as a μ-TAS to improve the movement of droplets. Fig. 2(a) shows the dimensions of the arrayed micro-pillars as projections, formed on a silicon (Si) substrate by the MEMS technique, and Fig. 2(b) shows the photograph of the fabricated projections. The arrow in the figure indicates the moving direction of the droplets. The gap was equal in the moving direction of the droplet and the orthogonal direction. Specifications of the pillars list are in Table 1. The projection was a 15 μm square, and the height was about 20 μm [32,34]. The cross-section of the pillar was square. The ratio of the area of all the pillars to the area of the substrate was defined as the area ratio of the

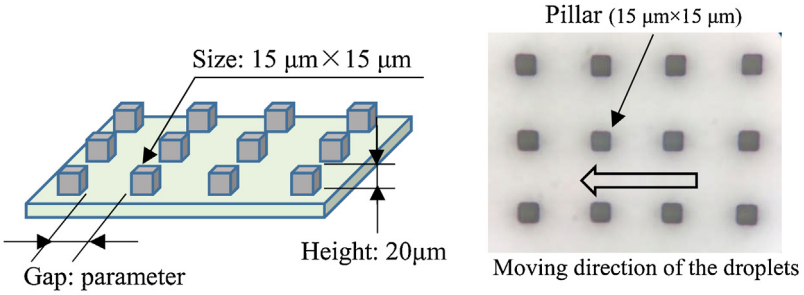

(a) Dimensions of the pillars (b) Photograph of the fabricated projections

Fig. 2. Dimensions of micro pillars.

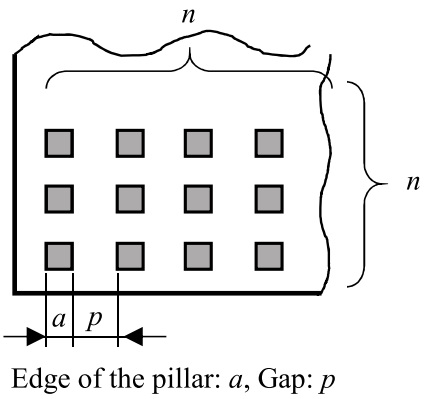

Fig. 3. Definition of area ratio. The area ratio was calculated from the pillar size and the gap: $(n^2 \times a^2) / (n \times a + (n\text{-}1) \times p)^2$, where a: edge length of the pillar, p: gap between the pillars, and n: number of the pillars in the row or the column.

Table 2
Specifications of liquids used for droplets.

Liquid		Viscosity (mPa•s)	Surface tension (mN/m)
Water		1.1	72.3
Glycerin[a] aqueous solution			
Concentration	20 wt%	2.1	70.7
	50 wt%	7.54	68.1
Ethanol[b] aqueous solution			
Concentration	2 wt%	1.12	63.0
	5 wt%	1.22	56.9
	17 wt%	1.31	51.1
	43 wt%	–	43.0

[a] No. 17018-25, NACALAI TESQUE INC.
[b] No. 14033-00, KANTO CHEMICAL CO. (Japan).

projection (hereinafter referred to as the area ratio) as shown in Fig. 3. Projections were formed by dry etching of silicon (Si). Silicon has a contact angle of approximately 65° with water, and is higher than glass, which is often used as a substrate of a microfluidic device [2–4]. Therefore, the performance of the Si substrate might appear somewhat higher than glass.

The liquid of the droplet was mainly water. Liquids other than water were also used to investigate the influence of viscosity and surface tension. The specifications of these liquids are shown in Table 2. The aqueous glycerol solution was used to change (increase) the viscosity. The range of viscosity was about 1 to 7 mPa·s (cf. viscosity of blood: approximately 4.7 mPa·s). The aqueous ethanol solution was used to change the surface tension. The surface tension was set to about 70 to 100% of water, because the acceleration was expected to become small when the surface tension was small. When changing the viscosity or the surface tension, the concentration was determined so that the surface tension or the viscosity did not change (cf. Table 2).

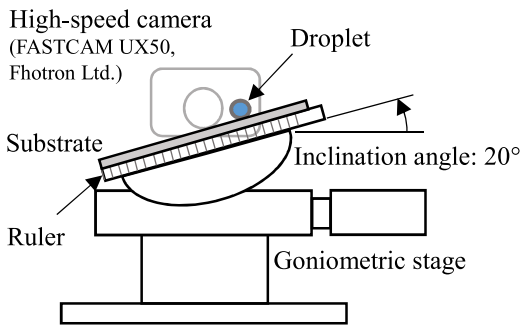

Fig. 4. Measurement apparatus used in this work.

Fig. 4 shows the measurement method for examining the dynamic characteristics of the droplets. The substrate was placed on the goniometer (the substrate was not electrically charged), and the behavior of the droplet on the inclined surface was observed with a high-speed camera from the side; then, the acceleration was calculated. In this work, the inclination angle was 20 °.

3. Result and discussion

3.1. Relationship between area ratio and sliding acceleration

It was reported that static contact angle was increased by making the pillar size smaller or enlarging the pillar gap [32,34]. This work introduced the area ratio of the projection to represent the density of the projections. When the area ratio was varied, the pillar size was fixed. The standard pillar size was determined to be 15 μm square. The gap of the pillars was used as well as the area ratio.

Fig. 5 shows the relationship between the static contact angle of the droplet (water) on the projection surface and the area ratio (a), and the relationship with the sliding angle when the droplet began to move by inclining the surface (b). The area ratio was varied in the range of 0.9 to 25%. When the area ratio was approximately less than 0.9%, most droplets fell down between the pillars, and no droplet was formed [34]. When the area ratio was 15% or less, the contact angle was more than 150° in the state of superhydrophobicity. When the area ratio was 21% or more, the pillar gap became almost equal to the pillar width, and the contact angle decreased to the latter half of 140°.

In the Cassie–Baxter model, the contact angle θ' is expressed by the equation: $\cos\theta' = f \times \cos\theta + f - 1$ (f: contact area ratio between the substrate and the liquid). In the Wenzel model, the contact angle

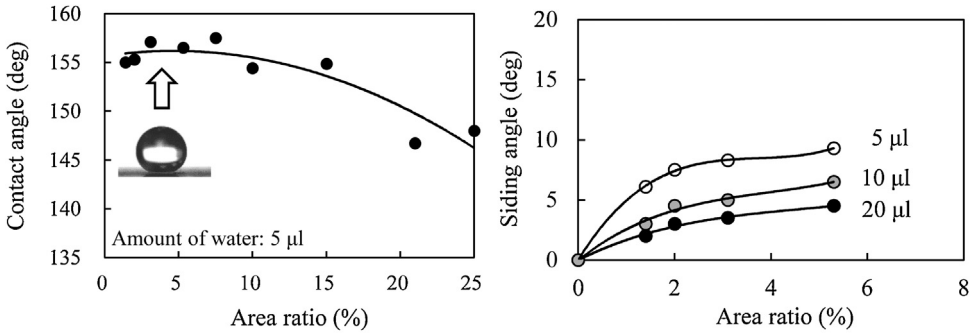

(a) Area ratio vs. contact angle (b) Area ratio vs. sliding angle

Fig. 5. Relationships between area ratio and static contact angle (a) and between area ratio and sliding angle (b).

θ ' is expressed by the equation: cos θ' = r × cos θ (r: roughness factor >1). The contact angle of water on the flat substrate (i.e., Si wafer) was θ = 65 °. The ratios f and r were 0.05 (5%) and 20, using the intermediate value of the area ratios. By substituting into the equation, the contact angle (θ') from the Cassie-Baxter model was 158 °. However, the Wenzel model could not be calculated because r was too large (cos θ' >1). The measured contact angles were in the range of 150 to 160 ° (cf. Fig. 5(a)). The amount of water in the measurement, to eliminate the influence of gravity, was 5 μl.

The sliding angle tended to decrease as the area ratio decreased (Fig. 5(b)). At the area ratio shown in the figure, the sliding angle is less than 10° (The sliding angle of the flat Si substrate was approximately 48° (10 μl)). For the area ratio in the range of 0.9–25%, and amount of liquid in the range of 5–20 μl in this work (φ2.1-3.4 mm, cf. capillary length of water: 2.72 mm), all the droplets were expected to slide down when the inclination angle was 20°. Therefore, the inclination angle (θ) of the substrate was set to 20°.

The measurement of acceleration in this work was conducted in the short distance, 10 mm to 30 mm from the beginning of movement, which was for use as a microfluidics device. The velocity range was also small (0.15-0.35 m/s). The equation of motion when a droplet moves on a slope is expressed as Eq. (1).

$$ma = mg\sin\theta - f \quad (1)$$

where m: mass of the droplet, a: acceleration, g: gravitational acceleration, θ: inclination angle, f: resistance force. The resistance forces, when the droplet moves on the slope, include friction on the contact surface, capillary force, viscosity of the liquid, and air resistance. These forces depend on the velocity of the droplet. In this work, the viscosity of the liquid and the air resistance were not considered to be significant because the velocity was small. The friction force and the capillary force were not expected to fluctuate significantly because the surface was extremely water-repellent. Therefore, the acceleration was considered to be roughly constant in the measurement conditions.

Fig. 6(a)–(c) shows the time histories of the measured displacement, velocity, and acceleration, respectively, after the droplet moves approximately 10 mm (volume: 10 μl, inclination: 20°, area ratio: 2%, 10%, and 21%). The displacement was measured at time intervals of either 0.005 s or 0.01 s. The velocity and acceleration were calculated by the time difference of the displacement and the velocity. This measurement was conducted several times, and the average acceleration was used. The velocity increased almost linearly. While there was some variation, the acceleration was roughly constant.

The projection is assumed to have caused an intermittent movement of the droplet owing to the pinning effect of projection. Some intermittent movements were observed in the time histories of the velocity and acceleration. However, it could not be determined if these movements were caused by the pinning effect. It is necessary to examine further how intermittent motion affects the acceleration.

Fig. 6(d) shows the behaviors of the droplets moving on the slope and the trajectories of the points on the droplet surfaces obtained by image processing. From these figures, the behavior of the droplets was considered to be mainly slip, probably because the moving distance after the start of movement was small (less than 30 mm).

Fig. 7(a) shows the relationship between the area ratio and the acceleration when the droplet slid down the inclined surface (pillar size: 15 μm square, inclination: θ = 20°). The measurement of acceleration was conducted in the displacement range of 10 to 30 mm from the beginning of movement as shown in Fig. 6(a). When the droplet was placed on the slope in the experiment, it was prevented from bouncing. Regarding the deformation of moving droplets, the displacement at the tip of the contact surface was used to measure the displacement. Variations of the measured acceleration

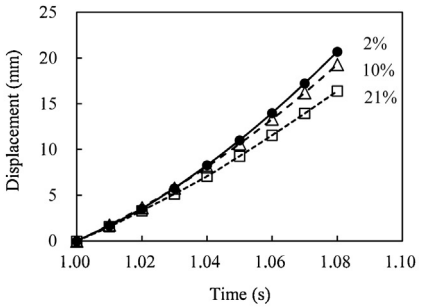

(a) Displacement (10 μl, Inclination: 20°, Area ratio: 2, 10, and 21 %)

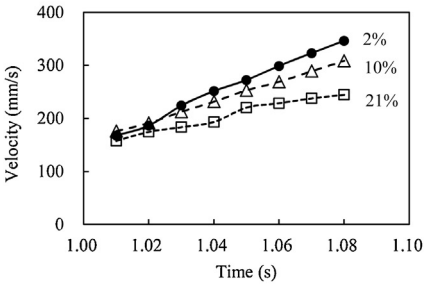

(b) Velocity (10 μl, Inclination: 20°, Area ratio: 2, 10, and 21 %)

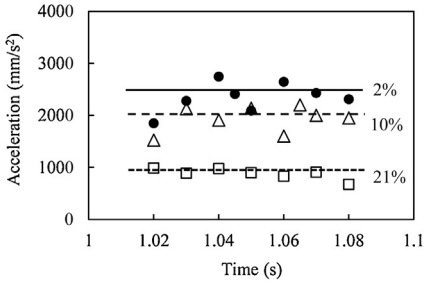

(c) Acceleration (10 μl, Inclination: 20°, Area ratio: 2, 10, and 21 %)

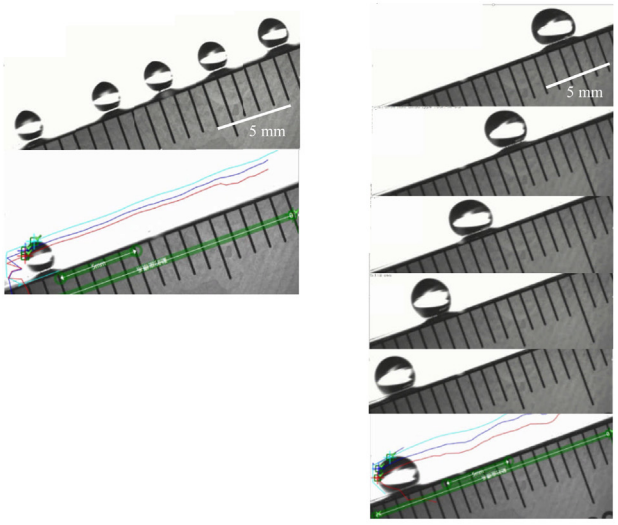

(d) Moving behaviors of the droplets (5 μl (left) and 20 μl (right), area ratio: 5.3%)

Fig. 6. Time histories of displacement, velocity, and acceleration of the droplets moving on the projection surfaces (a)-(c), and behaviors and trajectories of the droplets (d) (sliding length: about 20 mm, 1000 fps).

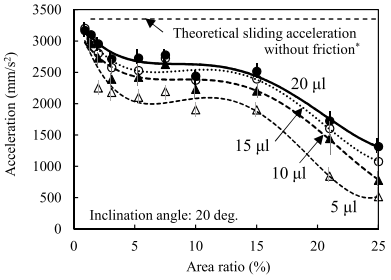

(a) Area ratio vs. acceleration (pillar size: 15 µm square)

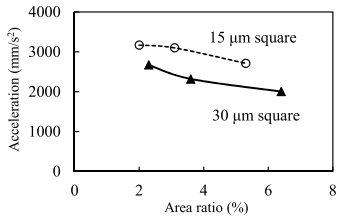

(b) Area ratio vs. acceleration (pillar size: 15 and 30 µm square, volume: 20 µl)

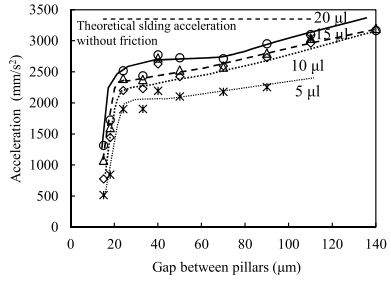

(c) Gap vs. acceleration (pillar size: 15 µm square)

Fig. 7. Relationships between area ratio and acceleration. Pillar size: 15 µm square (a) and 15 and 30 µm square (b). Figure (c) shows the relationship between the gap and the acceleration, where the area ratio of (a) is changed to the gap. (Inclination angle: 20 deg. Sliding acceleration without friction is 3350 mm/s^2.)

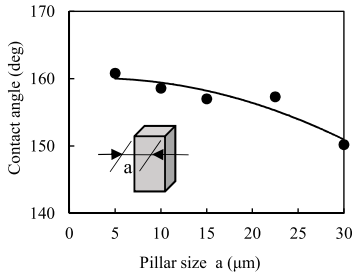

(a) Pillar size vs. contact angle

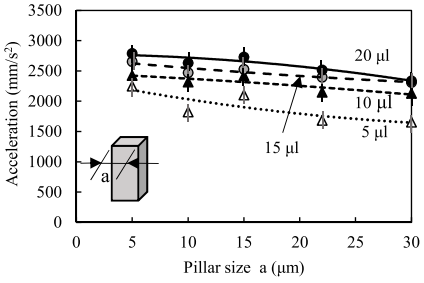

(b) Pillar size vs. acceleration (Area ratio: 6%, constant)

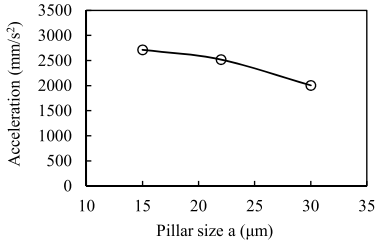

(c) Pillar size vs. acceleration (gap: 70 µm, constant, volume: 20 µl)

Fig. 8. Relationship between pillar size and static contact angle (a), and relationship between pillar size and acceleration ((b) and (c)). The area ratio was set to be constant at 6 % in (b) (the pillar gap was in the range of 20 to 90 µm). The pillar gap was set to be constant at 70 µm in (c) (the area ratio was in the range of 3 to 6 %).

are shown by the error bars. The figure indicates that acceleration increased with decreasing area ratios. This was probably because increased air was trapped between the pillars [16,25]. High accelerations were observed in the case of very small area ratios. When the area ratio was 1.4%, the acceleration was close to the sliding acceleration of a rigid body with no friction, approximately 3350 (mm/s^2) (= $g \times \sin\theta$, g: gravitational acceleration, θ: inclination angle of the substrate, 20°). However, when the area ratio was 0.9%, droplets fell down between the pillars. When the area ratio was between 5.3 to 15%, the acceleration slightly decreased as the area ratio increased. When the area ratio was about 21% or more, a large decrease occurred. When the area ratio was 30%, the sliding acceleration was expected to be close to zero. The pillar gap at the area ratio of 25% was almost the same as the pillar width (15 µm). For comparison, the pillar gap at the area ratio of 5.3% was about 3 times the pillar width. The droplet quickly slid when the area ratio was in the range of 1 to 15%. Thus, the area ratio considerably affected the acceleration. Fig. 7(b) shows the acceleration when the pillar size is 30 µm square (volume: 20 µl, inclination: 20°), as compared to Fig. 7(a) in which the pillar size is 15 µm square. The accelerations of the two pillar sizes changed almost similarly with respect to the area ratio.

The occurrence of three phases of the acceleration are displayed in Fig. 7(a). However, the reason for the acceleration not increasing significantly from 5% to 15% of the area ratio, is not completely clear. The following mechanism was expected. The droplet surface was suspended between the pillars with an area ratio less than approximately 15%, thereby reducing the mobility of the droplet. When the area ratio was less than 5%, a further decrease in the friction owing to a decrease in the contact area exceeded the above effect. Therefore, the acceleration increased again. The relationship between the acceleration and pillar gap was also examined by changing the area ratio in Fig. 7(a) to the pillar gap. Fig. 7(c) shows the result and it is slightly different from that of Fig. 7(a). It was concluded that the three phases were affected by the parameter. The mechanism of the three phases and the effect of these parameters require further investigation.

Fig. 8 shows the relationship between pillar size (width: a) and static contact angle (a) and acceleration (b). The area ratio of projections was set to be constant (approximately 6%). When the pillar width was decreased, the gap (b) between the pillars decreased; for example, b = 16 µm at a = 5 µm, b = 50 µm at a = 15 µm, and b = 92 µm at a = 30 µm. The variations of the measured acceleration are indicated by the error bars. The contact angle increased with the decrease in pillar size in Fig. 8(a). Fig. 8(b) indicates that the sliding acceleration increased as the pillar size decreased. Fig. 8(c) shows the acceleration when the pillar size changed at a constant pillar gap (70 µm), as compared to Fig. 8(b), in which the pillar size changed at a constant area ratio (6%). The area ratio and the pillar gap in both cases were almost in the same range (the gap in Fig. 8(b) ranges from 20 to 90 µm, and the area ratio in Fig. 8(c) ranges from 3% to 6%). The acceleration in both cases increased with a decrease in the pillar size. However, it was observed that the changes in the accelerations were quantitatively different.

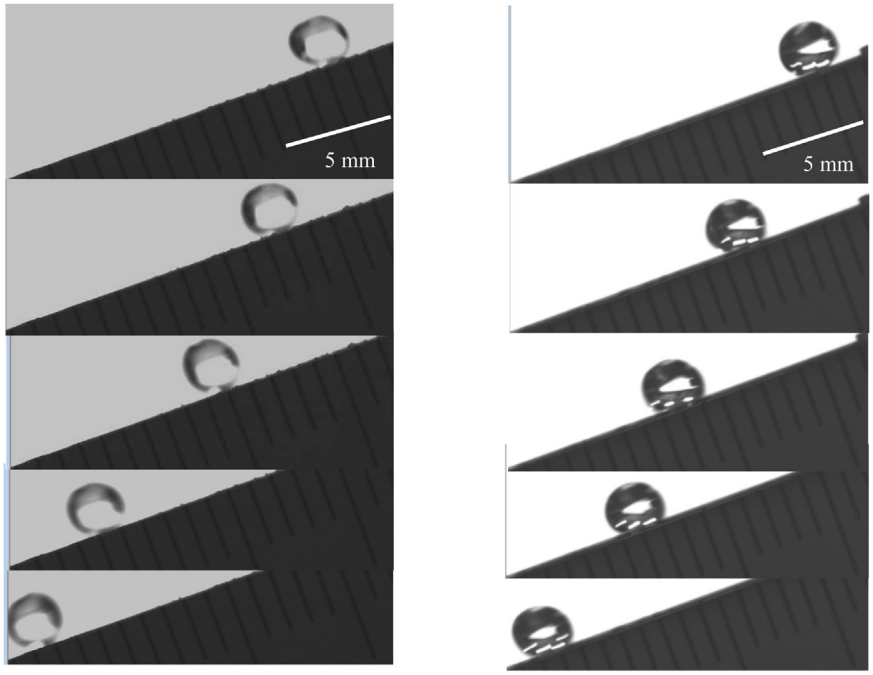

Fig. 9. Behaviors of droplets (10 μl) in the case of the different area ratios (1.4 and 21%, sliding length: about 20 mm, 1000 fps).

3.2. Behavior of droplet and sliding acceleration by calculation

Fig. 9 shows the behavior of sliding droplets captured with a high-speed camera. The area ratios are 1.4% (a) and 21% (b), and the liquid volume was 10 μl. The measured distance was approximately 20 mm. The area ratios almost corresponded to the smallest and the largest cases. The droplet at the area ratio of 1.4% was closer to a true sphere, and the droplet at the area ratio of 21% was slightly flat. The images suggest that the behavior of droplets was close to just slipping with a sphere shape. In addition, the contact surface of the droplet at the area ratio of 1.4% was small. Therefore, the sliding acceleration was probably close to the acceleration without friction (3350 mm/s^2) (cf. Fig. 7(a)). Conventional studies reported that the sliding mode was mainly caused when the static contact angle was large, and then a uniform acceleration motion was generated [38,39]. Because the contact angle was more than 150° (cf. Fig. 5(a)), the behavior of the droplet was considered to be almost sliding.

Furmidge's equation expresses the balance between the gravity component of the droplet in the inclined direction and the capillary force [44]. The latter approximately represents the friction of the contact surface when the droplet moves on the slope. Carre's equation, Eq. (2), is derived from Furmidge's equation by assuming the contact surface is a circle [45]. As the assumption of Eq. (2), resistance forces such as the moment when the droplet rotates, the internal flow resistance due to viscosity, and air resistance are ignored. For water-repellent surfaces, the contact surface is considered to be almost a circle. Therefore, Eq. (2) was used to compare with the measurement in this work.

$$ma = mg\sin\theta - 1/2 \bullet \pi\gamma_{lv} \bullet r(\cos\theta_R - \cos\theta_A) \quad (2)$$

where γ_{lv} is surface tension of liquid contacting with air (72.8 mN/m), r is the contact radius, and θ_A and θ_R are the advancing and receding contact angles. In Eq. (2), the first term on the right side is the component of gravity in the slope direction, and the second term is the friction force. The contact area of the droplet in the experiment could be assumed to be almost a circle because the droplet was almost spherical (cf. Fig. 9).

Table 3
Hysteresis and contact radius[a].

Area ratio (%)	Hysteresis $\theta_A - \theta_R$ (deg)	Contact radius r (mm)
2.0	6.1	0.691
3.1	9.0	0.534
5.3	7.1	0.569
10	7.1	0.885
21	13.1	0.790

[a] Droplet: water, 10 μl.

Fig. 10(a) shows the relationship between the area ratio and the measured advancing and receding contact angles (droplet: 10 μl ($m = 10^{-5}$ kg)). Variations of the angles are shown by the error bars. The hysteresis and the contact radius are shown in Table 3. Because the droplet was almost spherical, the hysteresis was a small value less than 10°. The smaller area ratio roughly had a larger dynamic contact angle and a smaller contact radius. Fig. 10(b) shows the acceleration calculated by using Eq. (2). The figure indicates that as the area ratio decreased, the acceleration increased. This was considered to be due to the increase in the dynamic contact angle (θ_A, θ_R) and the decrease in the contact radius (r) in Eq. (2). When the area ratio was approximately less than 3%, the calculation almost agreed with the measurement. This suggested that the behavior of the droplet was almost sliding at the low area ratio. The difference between them became large when the area ratio was large. The fluctuation of the contact angle of the droplet became large due to swaying of the droplet. The average value was used in Fig. 10. This variation was considered to be main cause of the error.

3.3. Influence of hydrophobicity and hydrophilicity of substrate

Silicon (Si) substrate was used in the experiments. However, glass and other materials are used for various applications. Therefore, the static contact angle and sliding acceleration when the

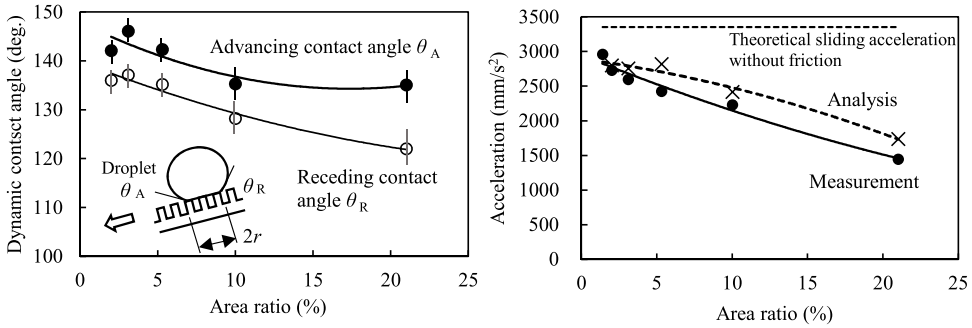

(a) Advancing and receding contact angles. (b) Analytical and measured sliding acceleratio

Fig. 10. Measured dynamic contact angles (a) and sliding accelerations by calculation using dynamic contact angle and contact radius (b) (droplet: 10 μl).

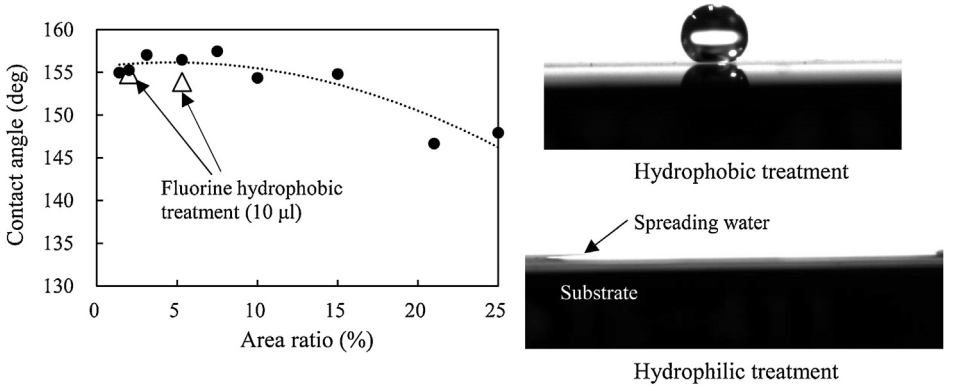

(a) Static contact angle (b) Droplets on the surfaces with different treatments

Fig. 11. Relationships between area ratio and contact angle when hydrophobic treatment was conducted (a). Droplet was not formed on the surface with hydrophilic treatment (b): water spread on the surface.

Table 4
Processing conditions of hydrophobic and hydrophilic treatments.

Hydrophobic treatment: CF_4 plasma[a]	
CF_4 gas: 50 sccm	Pressure: 100 Pa
Power: 50 W	Processing time: 1 min.
Hydrophilic treatment: O_2 plasma[a]	
O_2 gas: 50 sccm	Pressure: 100 Pa
Power: 50 W	Processing time: 1 min.

The contact angles of water droplets on a flat Si substrate were 110° (hydrophobic treatment) and 8° (hydrophilic treatment).

[a] Apparatus: CPE-200A, SAKIGAKE-Semiconductor Co. (Japan).

Table 5
Acceleration in the case with and without hydrophobic treatment.

Area ratio (%)	2.0	5.3
No treatment (mm/s²)	2732[a], 2954[b]	2426, 2730
With treatment (mm/s²)	2898, 3015	2460, 2702

[a] 10 μl.
[b] 20 μl.

hydrophobicity and hydrophilicity of the substrate changed were investigated. Hydrophobic treatment using fluorine plasma and hydrophilic treatment using oxygen plasma were performed to the substrate. The processing conditions are shown in Table 4. The area ratios of the substrates were 2% and 5.3%.

Fig. 11(a) show the static contact angles of the water droplet (10 μl) on the substrate with the hydrophobic treatment (photograph: Fig. 11(b) (left)). The contact angle did not change significantly. It was reported that using only the chemical treatment to decrease surface energy did not realize a static contact angle exceeding 115° [5,6]. Therefore, it was considered that the contact angle did not increase much because the original contact angles exceeded 150°. For the Si substrate without projection, the contact angles were 110° (hydrophobic treatment) and 8° (hydrophilic treatment) after the treatments. In addition, the change of the sliding accelerations was also slight, as shown in Table 5.

On the other hand, for the substrates with the hydrophilic treatment, the droplet could not be formed for both substrates because the droplet was spread immediately, as shown in Fig. 11(b) (right). Because this treatment was completed in a short time, it was impossible to change the degree of hydrophilization. The contact angle of the water droplets in a silicon substrate was approximately 65°. When the material of a substrate has a smaller static contact angle, the performance, as shown in Fig. 7(a), would decline. As a measure against this, it would be effective to provide the hydrophobic treatment to the surface.

3.4. Influence of viscosity and surface tension of droplet

3.4.1. Viscosity

The sliding acceleration was examined when the viscosity and the surface tension of the droplet were changed. The acceleration was examined in the low area ratio less than 5.3% (cf. Fig. 7(a)). This was to enhance the acceleration of the droplets with high viscosity or low surface tension by optimizing the area ratio. The velocity of the droplet was in the order of several m/s; therefore, the influence of the viscosity was considered [33]. The specifications of the liquid used are listed in Table 2. The concentration was changed in glycerin and ethanol aqueous solutions.

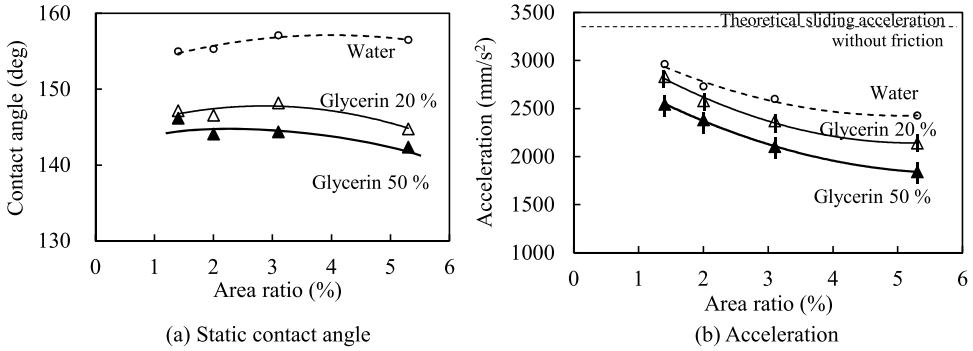

Fig. 12. Relationship between area ratio and static contact angle (a) and acceleration (b) when viscosity of liquid was varied (droplet: 10 μl).

Table 6
Forming a droplet on projection surfaces.

Surface tension (mN/m)	Area ratio (%) 1.4	2.0	…	25	30
51 or more	○	○		○	○
From 43 to 51	×	○		○	○
43	×	○		○	×

Fig. 12(a) shows the static contact angle and Fig. 12(b) shows the relationship between the area ratio and sliding acceleration of the droplets (10 μl) when viscosity was varied. Variations of measured acceleration are indicated by the error bars. As the viscosity increased, the contact angle and the acceleration decreased. The decrease in acceleration against viscosity was roughly proportional to approximately -0.10 power of viscosity. While the reason why the acceleration decreased as the viscosity increased was not fully clear, the flow resistance on the contact surface and inside the droplet was considered to be one of the causes [33,42,43]. The reason why the contact angle decreased with increasing viscosity was also not clear, the adhesion to the projection due to the viscosity might be affected.

3.4.2. Surface tension

As for surface tension, the droplets fell down between the pillars at a small area ratio when the surface tension was sufficiently small. When the surface tension was less than 51 mN/m (ethanol aqueous solution more than 17 wt%), the droplet (10 μl) fell down between the pillars at an area ratio of 1.4% (pillar gap: 110 μm). When the surface tension was 43 mN/m (ethanol aqueous solution of 43 wt%), the droplet (10 μl) spread on the pillar surface at an area ratio of 30% (pillar gap: 12 μm). These statistics are summarized in Table 6. In these experiments, the pillar size was 15 μm square and the substrate was placed horizontally. The lower limit of the surface tension at which droplets are formed depends on the area ratio. The lower the area ratio, the higher the limit. This was probably derived from that the droplet surface could not hang between the pillars. These characteristics are determined by the surface tension, the Laplace pressure of the liquid, and the gravity of the droplet. When the area ratio is 1.4%, the lower limit of the surface tension was 51 mN/m (cf. Table 2). When the surface tension of the droplet is small, it is difficult to achieve an area ratio that is small enough. As a measure against this, it would be effective to reduce the size of the pillar to enhance the acceleration (cf. Fig. 8(b)).

Fig. 13(a) shows the contact angle and Fig. 13(b) shows the relationship between the area ratio and the acceleration of the droplets (10 μl) when the surface tension was varied. As the surface tension decreased, the contact angle and the acceleration declined. The decrease in acceleration was roughly proportional to the surface tension at approximately 0.59 power. When the surface tension was small, the shape of the droplet became flattened due to gravity; the contact surface became large. In addition, it was expected that the surface between the pillars was greatly deflected. These might be the reasons for the decrease of the acceleration.

The cause of the decrease in the acceleration when the viscosity and the surface tension are varied (cf. Figs. 12(b) and 13 (b), respectively), was investigated based on the dynamic contact angle and the contact radius. Fig. 14(a) and (b) show the dynamic contact angle and the contact radius of a 50% aqueous glycerol solution and a 5% ethanol aqueous solution (10 μl), respectively. In the photographs shown in Fig. 14(c) and (d), which show the behavior of the droplets, both droplets were slightly flat during sliding (area ratio: 5.3%). These figures suggest that the behavior of the droplet was almost sliding. Fig. 14(a) and (b) show that the dynamic contact angle decreased with an increase in the viscosity or a decrease in the surface tension, respectively. The contact radius also increased. These are also considered to affect the decrease in the acceleration, based on the analogy presented in Fig. 10.

Fig. 12(b) and 13 (b) show that lowering the area ratio is useful for increasing the sliding acceleration, even for a solution with a high viscosity or low surface tension. A glycerin droplet (10 μl) with a high viscosity (viscosity: 1410 mPa-s, surface tension: 63 mN/m), can slide down the surface with an area ratio of 5.3% (inclination angle: 20°).

3.4.3. Further investigation of viscous droplets

For a droplet with high viscosity, the contact boundary between the droplet and the substrate is no longer a circle, i.e., Carre's equation (Eq. (2)) does not hold. Therefore, the equation of motion of a viscous droplet is considered based on Carre's equation. The resisting force per unit length on the contact boundary of the droplet in Carre's model is expressed as follows [45].

$$f = \frac{1}{2}\gamma_{lv}\left(\cos\theta_R - \cos\theta_A\right) = f_R - f_A$$

The dynamic contact angles θ_R and θ_A of the viscous droplet on a slope depend on the angular position of φ in Fig. 15(a). Therefore, the equation of motion of the droplet is considered to be Eq. (3). The second and third terms on the right side of Eq. (3) represent the movement direction component of the surface tension (γ) on the contact boundary.

$$ma = mg\sin\theta - \frac{1}{2}\gamma_{lv}\left(\int_{AB}\int_0^{\pi}\cos\theta_R \sin\varphi d\varphi ds - \int_{CD}\int_0^{\pi}\cos\theta_A \sin\varphi d\varphi ds\right) \quad (3)$$

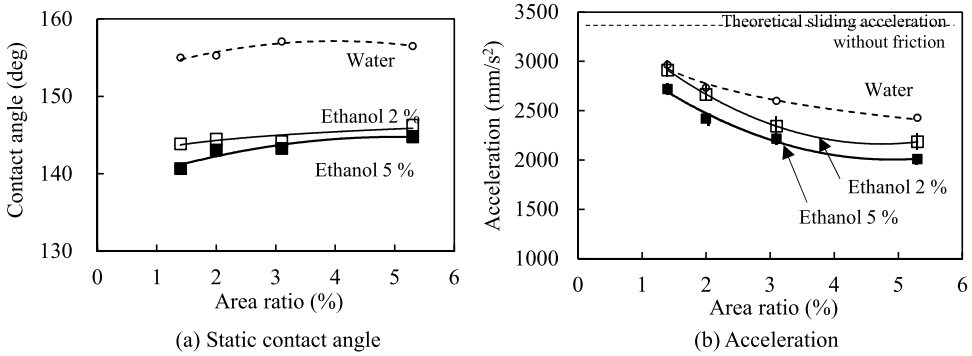

Fig. 13. Relationship between area ratio and static contact angle (a) and acceleration (b) when surface tension of liquid was varied (droplet: 10 μl).

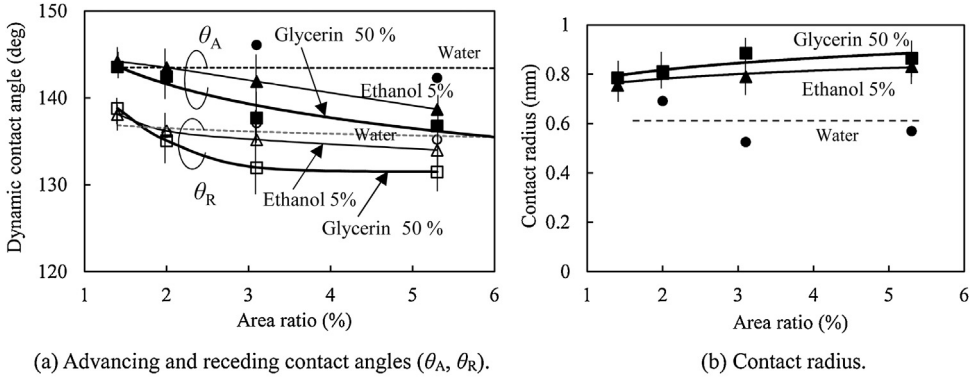

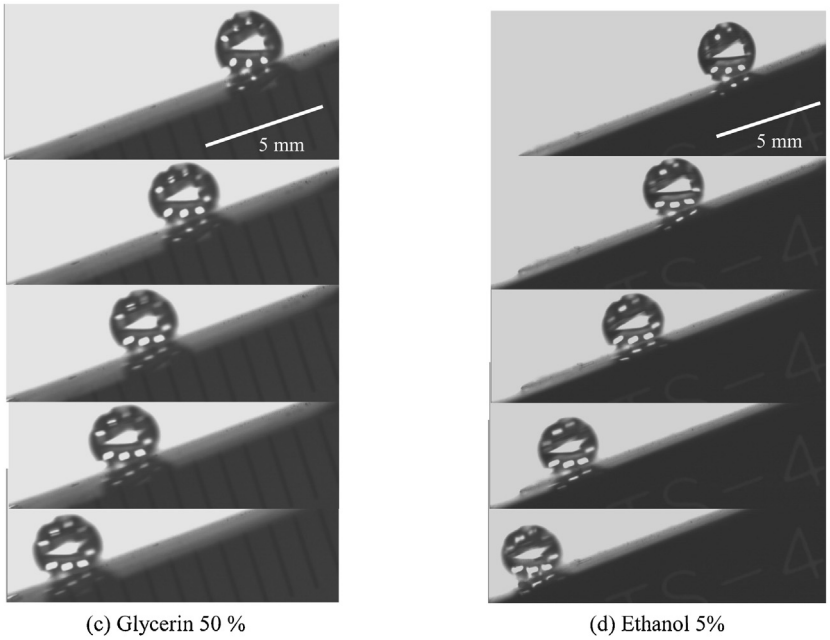

Fig. 14. Relationships between area ratio and dynamic contact angle (a) and contact radius (b) of liquid with different viscosity and surface tension (droplet: 10 μl). Moving behaviors of droplets (c) and (d).

where the variables are the same as Eq. (2). "sin φ" of the second and third terms on the right side is for obtaining the movement direction component of the surface tension and the component is summed by the integral (ds).

Equation (3) needs to grasp the accurate shape of the contact boundary and the dynamic contact angles. However, because determining these is difficult, the following simple model was used to discuss the experimental results of Fig. 14: the changes of contact radius (r) and the contact angle (θ) were examined. The acceleration was calculated by substituting the above values to Carre's equation and the acceleration was compared with the measured acceleration. Then which factor affected the error was examined.

The height of the glycerin 50% droplet (h_1) was smaller than the height of the water droplet (h_0) ($h_1 < h_0$, cf. Figs. 14(c) and 9 (a)). On the other hand, the contact radius of the glycerin 50% droplet (r_1) was larger than that of the water droplet (r_0) ($r_1 > r_0$). The contact

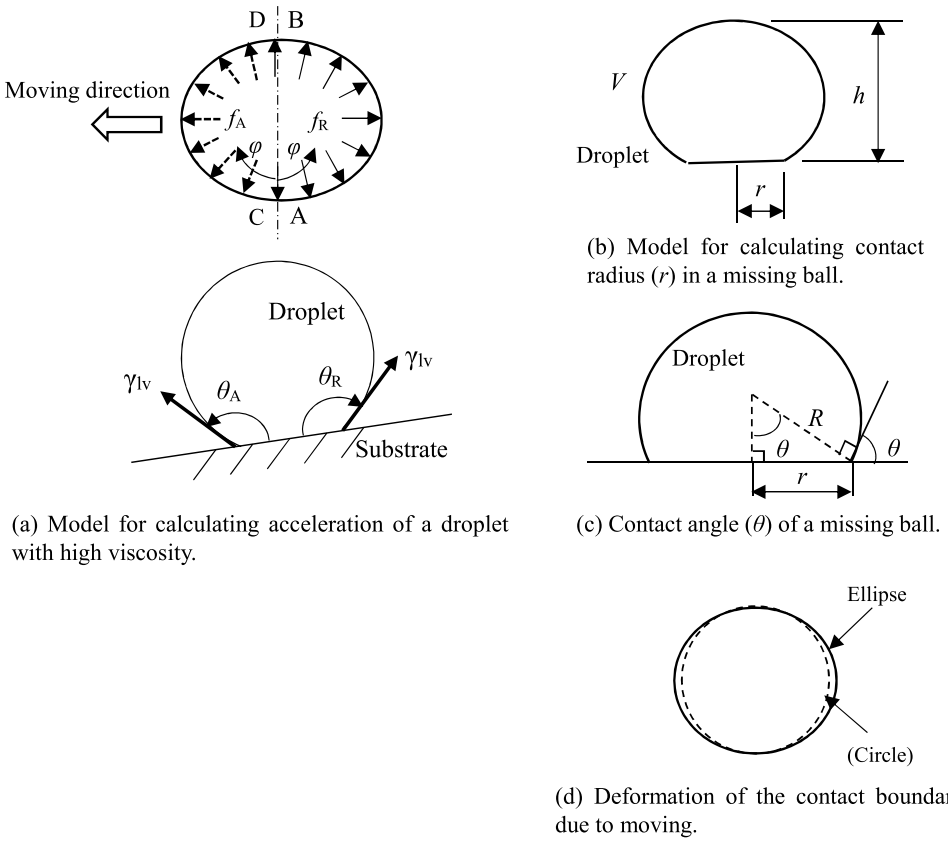

(a) Model for calculating acceleration of a droplet with high viscosity.

(b) Model for calculating contact radius (r) in a missing ball.

(c) Contact angle (θ) of a missing ball.

(d) Deformation of the contact boundary due to moving.

Fig. 15. Model to calculate the resisting force acting on the contact boundary of the droplet (a) and the model for calculating the contact radius and the contact angle by using a missing ball (b) and (c), respectively.

radius of r_1 can be calculated roughly by Eq. (4) from the volume of the missing ball of Fig. 15(b), while this value represents a static case.

$$V = \left(\pi h_0/6\right) \times \left(3r_0^2 + h_0^2\right) = \left(\pi h_1/6\right) \times \left(3r_1^2 + h_1^2\right) \quad (4)$$

The values of h and r of the droplets (10 μl) in Fig. 15(b) were determined from Figs. 9 and 14: water droplet: h_0 = 2.53 mm, r_0 = 0.6 mm; glycerin 50% droplet: h_1 = 2.38 mm. The value of r_1 of the glycerin droplet was obtained as 0.87 mm. This almost coincided with the result shown in Fig. 14(b).

The Reynolds number (Re = $\rho V \cdot r / \mu$, ρ: density, V: velocity, r: contact radius, μ: viscosity) was calculated to be approximately 26 for the glycerin 50% droplet of 10 μl (ρ: 1130 kg/m^3, V: 0.2 m/s (cf. Fig. 6(b)), r: 0.86 × 10^{-3} m (cf. Fig. 14), μ = 7.54 mPa· s (cf. Table 2)). The reason for that the calculated contact radius almost coincided with the measurement is probably due to the fact that the Reynold number was small. Conventional studies have shown the contact radius in the case of dropping the viscous droplet on the plane and the contact radius increased approximately 1.15 times at the same Reynold number [46–48]. That is, the change of the contact radius was small.

The contact angle in the above case was obtained as $180^\circ - \theta$ from the geometrical relationship in Fig. 15(c). The contact angle is obtained as about 140 ° by using the measured values of r_1 and R_1 of the glycerin 50% solution, 0.86 mm and 1.35 mm, respectively ($\theta = \sin^{-1}(r_1 / R_1)$). The measured values (cf. Fig. 14(a)) were a slightly different (θ_A = 139 ° and θ_R = 131°). It is because the change of the contact angle due to the inclination of slope and the dynamic behavior of the droplet is not taken into consideration. The dynamic contact angle is expected to decrease due to the energy loss by viscosity. However, the value of Weber number (We = $\rho V^2 \cdot r / \gamma$, γ: surface tension, cf. Table 2)) of the droplet was approximately 0.5. According to this small Weber number, it is considered that large deformation is suppressed [46–48].

By substituting the contact radius and contact angle (r_1 = 0.86 mm, θ_A = 139 °, and θ_R = 131°, cf. Fig.14 (a) and (b)) of the 50% glycerin droplet into Carre's equation, the calculated acceleration was approximately 2200 mm/s^2. This was 10 - 15% larger than the measured value (1900 −2000 mm/s^2, cf. Fig. 12(b)). This difference was considered to be due to the change of the contact boundary by the effect of viscosity (Carre's equation assumes it as a circle). When the viscosity was high, the contact boundary was expected as an ellipse when the droplet moved on the slope. This effect enlarges the resisting force of the right side of Eq. (2) because the contact boundary is enlarged as shown in Fig. 15(d). The calculated acceleration roughly agreed with the experimental result when the expansion factor ("c" in Eq. (2')) was 1.15.

$$ma = mg\sin\theta - 1/2 \bullet \pi\gamma_{lv} \bullet r(\cos\theta_R - \cos\theta_A) \bullet c \quad (2')$$

In the above estimation, the difference between the calculated acceleration and the measured acceleration is considered to be due to the shape of the contact boundary. To incorporate the accurate shape of the contact boundary into Eq. (3) is considered to improve the accuracy.

4. Conclusions

The sliding acceleration in the method of transporting liquid droplets by inclined surfaces (20°) provided with fine projections (area: 15 μm square, height: 20 μm) was investigated by introducing the area ratio of projections from 0.9% to 25%. The contact angle of the water droplets on the projection surface was approximately 155°. The sliding acceleration increased with the decrease

in the area ratio. When the area ratio was 2% or less, it was close to the theoretical sliding acceleration with no friction. When the area ratio was less than 1%, the droplets fell down between the projections. When the area ratio was more than 21%, the acceleration was greatly reduced. Therefore, the effective area ratio ranged from 1 to 15%. Because the droplet slide maintains an almost spherical shape in the case of very low area ratio, the measured acceleration almost corresponded with the acceleration calculated by using dynamic contact angle. Lowering the area ratio was useful for increasing the sliding acceleration, even for a solution with high viscosity or low surface tension. It was apparent that the acceleration was almost controlled by the area ratio of projection.

Declaration of Competing Interest

There is no conflict of interest in this paper.

References

[1] D.J. Harrison, K. Fluri, K. Seiler, Z. Fan, C.S. Effenhauser, A. Manz, Micromachining a Miniaturized Capillary Electrophoresis-Based Chemical Analysis System on a Chip, Science 261 (5123) (1993) 895–897.
[2] Y. Temiz, R.D. Lovchik, G.V. Kaigala, E. Delamarche, Lab-on-a-chip devices: How to close and plug the lab? Microelectronic Engineering 132 (2015) 156–175.
[3] M.I. Mohammeda, S. Haswellb, I. Gibsona, Lab-on-a-chip or Chip-in-a-lab: Challenges of commercialization lost in translation, The International Design Technology Conference, DesTech2015, Procedia Technology 20 (2015) 54–59.
[4] B. Yılmaz, F. Yılmaz, Lab-on-a-Chip Technology and Its Applications, in: Omics Technologies and Bio-Engineering, Academic Press, 2018, pp. 145–153.
[5] A. Nakajima, Designing of super hydrophobic coatings, Ceramics 37 (3) (2002) 148–151 (in Japanese).
[6] A. Nakajima, K. Hashimoto, T. Watanabe, Present state of super hydrophobic coatings, PETROTECH 25 (4) (2002) 22–26 (in Japanese).
[7] K. Honda, M. Morita, H. Otsuka, A. Takahara, Molecular Aggregation Structure and Surface Properties of Poly (fluoroalkyl acrylate) thin Films, Macromolecules 38 (13) (2005) 5699–5705.
[8] T. Morimoto, Y. Sanada, H. Tomonaga, Wet chemical functional coatings for automotive glasses and cathode ray tubes, Thin Solid Films 392 (2) (2001) 214–222.
[9] K. Honda, M. Morita, O. Sakata, S. Sasaki, A. Takahara, Effect of surface molecular aggregation state and surface molecular motion on wetting behavior of water on poly (fluoroalkyl methacrylate) thin Films, Macromolecules 43 (2010) 454–460.
[10] N. Yoshida, Y. Abe, H. Shigeta, A. Nakajima, H. Ohsaki, K. Hashimoto, T. Watanabe, Sliding behavior of water droplets on flat polymer surface, Amer. Chem. Soc. 128 (3) (2006) 743–747.
[11] T. Taniguchi, T. Torii, T. Higuchi, Micro chemical reactor in micro droplet, Electrostatic manipulation of micro droplet, Proc. TSMM (2001) 104–105.
[12] Z. Wang, L. Ci, L. Chen, S. Nayak, P. Ajayan, N. Koratkar, Polarity-dependent electrochemically controlled transport of water through carbon nanotube membranes, Nano Lett. 7 (3) (2007) 697–702.
[13] T. Wu, Y. Suzuki, N. Kasagi, Electrostatic droplet manipulation using electret as a voltage source, MEMS (2008) 591–594.
[14] J. Li, Y. Wei, Z. Huang, F. Wang, X. Yan, Investigation of the electric field driven self-propelled motion of water droplets on a super-hydrophobic surface, IEEE Trans, Dielectrics and electrical insulation 23 (5) (2016) 3007–3015.
[15] S. Li, X. Ding, F. Guo, Y. Chen, M. Lapsley, S. lin, L. Wang, J.M. Cameron, T. Huang, An on-chip, multichannel droplet sorter using standing surface acoustic waves, Analy. chemistry 85 (11) (2013) 5468–5474.
[16] Z. Yoshimitsu, A. Nakajima, T. Watanabe, K. Hashimoto, Effects of surface structure on the hydrophobicity and sliding behavior of water droplets, Langmuir 18 (15) (2002) 5818–5822.
[17] A. Nakajima, S. Suzuki, Y. Kameshima, N. Yoshida, T. Watanabe, K. Okada, Sliding mode transition of water droplet on the silicon surface coated with octadecyltrichlorosilane, Chem. Lett. 32 (12) (2003) 1148–1149.
[18] S. Suzuki, A. Nakajima, Y. Kameshima, K. Okada, Elongation and contraction of water droplet during sliding on the silicon surface treated by fluoroalkylsilane, Surface Sci. Lett. 557 (2004) 163–168.
[19] J.W. Ha, I.J. Park, S.B. Lee, Hydrophobicity and sliding behavior of liquid droplets on the fluorinated latex films, Macromolecules 38 (3) (2005) 736–744.
[20] M. Sakai, J.-H. Song, N. Yoshida, S. Suzuki, Y. Kameshima, A. Nakajima, Direct observation of internal fluidity in a water droplet during sliding on hydrophobic surfaces, Langmuir 22 (11) (2006) 4906–4909.
[21] E. Bormashenko, Y. Bormashenko, G. Oleg, On the nature of the friction between nonstick droplets and solid substrates, Langmuir 26 (15) (2010) 12479–12482.
[22] A. Nakajima, Y. Nakagawa, T. Furuta, M. Sakai, T. Isobe, S. Matsushita, Sliding of water droplets on smooth hydrophobic silane coatings with regular triangle hydrophilic regions, Langmuir 29 (29) (2013) 9269–9275.
[23] R.N. Wenzel, Resistance of solid surfaces to wetting by water, Ind. Eng. Chem. 28 (1936) 988–994.
[24] A.B.D. Cassie, S. Baxter, Wettability of porous surfaces, Trans. Faraday Soc. 40 (1944) 546–551.
[25] M. Miwa, A. Nakajima, A. Fujishima, K. Hashimoto, T. Watanabe, Effects of surface roughness on sliding angles of water droplets on superhydrophobic surfaces, Langmuir 16 (13) (2000) 5754–5760.
[26] A. Nakajima, M. Hoshino, J.-H. Song, Y. Kameshima, K. Okada, Effect of roughness on lipophobicity of a surface prepared using boehmite nanoparticles and fluoroalkylsilane, Chem. Soc. Japan 34 (7) (2005) 908–909.
[27] C. Dorrer, J. Ruhe, Drops on microstructured surface coated with hydrophilic polymers: Wenzel's model and Beyond, Langmuir 24 (5) (2008) 1959–1964.
[28] Y. Ando, T. Tanaka, J. Ino, K. Kakuta, Relation among friction and pull-off forces and surface geometry in nano meter-scale, Trans. JSME C 65 (637) (1999) 3784–3791 (in Japanese).
[29] Z. Burton, B. Bhushan, Hydrophobicity, adhesion and friction properties of nanopatterned polymers and scale dependence for micro-and nanoelectrochemical systems, Nano Lett. 5 (8) (2005) 1607–1613.
[30] Y.C. Jung, B. Bhushan, Contact angle, adhesion and friction properties of micro-and nanopatterned polymers superhydrophobicity, Nanotechnology 17 (19) (2006) 4970–4980.
[31] J. Yang, Z. Yang, C. Chen, D. Yao, Conversion of surface energy and manipulation of a single droplet across micropatterned surfaces, Langmuir 24 (17) (2008) 9889–9897.
[32] N. Moronuki, A. Takayama, A. Kaneko, Design of surface texture for the control of wettability, Trans. JSME B 70 (693) (2004) 126–131 (in Japanese).
[33] K. Suzuki, Flow resistance of a liquid droplet confined between two hydrophobic surfaces, Microsystem Technologies 11 (8-10) (2005) 1107–1114.
[34] S. Kobayashi, E. Makino, T. Mineta, Effects of dimension of micro pillar array plasma modification wetting properties of SU-8 surface for water droplets, J. Surf. Finish. Soc. Jpn. 62 (3) (2011) 184–188 (in Japanese).
[35] E. Martines, K. Seunarine, H. Morgan, N. Gadegaarde, C. Wilkinson, M. Riehle, Superhydrohobicity and superhydrophilicity of regular nanopatterns, Nano Lett. 5 (10) (2005) 2097–2103.
[36] N. Yoshida, Y. Abe, H. Shigeta, K. Takami, H. Osaki, T. Watanabe, K. Hashimoto, Preparation and water droplet sliding properties of transparent hydrophobic polymer coating by molecular design for self-organization, J. Sol-Gel Sci. and Tech. 31 (2004) 195–199.
[37] S. Gogte, P. Volobieff, Effective slip on textured superhydrophobic surfaces, Phys. of Fluid 17 (5) (2005), 051701.
[38] S. Suzuki, A. Nakajima, M. Sakai, J. Song, N. Yoshida, et al., Sliding acceleration of water droplets on a surface coated with fluoroalkylsilane and octadecyltrimethoxysilane, Surf. Sci. 600 (2006) 2214–2219.
[39] M. Sakai, J. Song, N. Yoshida, S. Suzuki, Y. Kameshima, A. Nakajima, Relationship between sliding acceleration of water droplets and dynamic contact angles on hydrophobic surfaces, Surf. Sci. 600 (2006) L204–L208.
[40] M.S. Ambrosia, M.Y. Ha, S. Balachandar, The effect of pillar surface fraction and pillar height on contact angles using molecular dynamics, Applied Surface Sci. 282 (2013) 211–216, Elsevier.
[41] S. Suzuki, A. Nakajima, M. Sakai, Y. Sakurada, N. Yoshida, A. Hayashi, Y. Kameshima, K. Okada, Slipping and rolling ratio of sliding acceleration for a water droplet sliding on fluoroalkyisilane coatings of different roughness, Chem. Lett. 37 (1) (2008) 58–59.
[42] M. Sakai, A. Hashimoto, N. Yoshida, S. Suzuki, Y. Kameshima, A. Nakajima, Image analysis system for evaluating sliding behavior of a liquid droplet on a hydrophobic surface, R. Sci. Inst. 78 (2007), 045103.
[43] Y. Sakurada, S. Suzuki, M. Sakai, A. Nakajima, Y. Kameshima, K. Okada, Effect of liquid viscosity on the internal fluidity of a droplet sliding on a fluoroalkylsilane coating, Chem. Lett. 37 (7) (2008) 688–689.
[44] C.G.L. Furmidge, Study at phase interface. I. The sliding of liquid drops on solid surfaces and a theory for spray retention, J. Colloid Sci. 17 (1962) 309–324.
[45] A. Carre, M.E.R. Shanahan, Drop motion on an inclined plane and evaluation of hydrophobia treatments to glass, Adhesion 49 (3/4) (1995) 177–185.
[46] J. Guo, S. Lin, B. Zhao, X. Deng, L. Chen, Spreading of impinging droplets on nanostructured superhydrophobic surfaces, Applied Physics Lett. 113 (2018), 071602.
[47] H.-M. Huang, X.-P. Chen, Energetic analysis of drop's maximum spreading on solid surface with low impact speed, Physics of Fluids 30 (2018), 022106.
[48] C. Antonini, A. Amirfazli, M. Marengo, Drop impact and wettability: From hydrophilic to superhydrophobic surfaces, Physics of Fluids 24 (2012), 102104.

Biography

Satomitsu Imai was born in 1961 in Chiba, Japan. He is a professor of department of Precision Machinery Engineering of College of Science and Technology, Nihon University (Japan). He has been engaged in developing micro mechanical actuators and their fabrication methods. He is interested in applying nano and polymer materials to MEMS.